



Published in final edited form as:

J Am Chem Soc. 2016 June 29; 138(25): 7860–7863. doi:10.1021/jacs.6b04686.

On- and Off-Cycle Catalyst Cooperativity in Anion-Binding Catalysis

David D. Ford[#], Dan Lehnerr[#], C. Rose Kennedy, and Eric N. Jacobsen^{*}

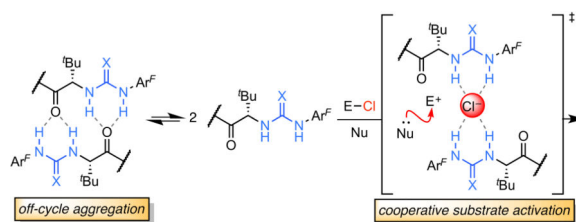
Department of Chemistry and Chemical Biology, Harvard University, Cambridge, Massachusetts 02138, USA.

[#] These authors contributed equally to this work.

Abstract

Chiral, neutral H-bond donors have found widespread use as catalysts in enantioselective reactions involving ion-pair intermediates. Herein, a systematic mechanistic study of a prototypical anion-binding reaction, the thiourea-catalyzed enantioselective alkylation of α -chloroethers, is detailed. This study reveals that the catalyst resting state is an inactive dimeric aggregate that must dissociate and then reassemble to form a 2:1 catalyst–substrate complex in the rate-determining transition structure. Insight into this mode of catalyst cooperativity sheds light on the practical limitations that have plagued many of the H-bond donor-catalyzed reactions developed to date and suggests design strategies for new, highly efficient catalyst structures.

Graphical abstract



Hydrogen-bond (H-bond) donors such as chiral urea, thiourea, and squaramide derivatives enjoy widespread application in a range of highly enantioselective transformations.¹ These catalysts have many desirable properties, including stability to air and moisture, comparatively low cost, and ease of synthesis from readily available building blocks. These systems were initially explored for the direct activation of neutral, Lewis basic electrophiles through a LUMO-lowering effect (Figure 1A).^{1,2} More recently, they have been increasingly applied for ion-pairing catalysis, wherein the chiral H-bond donor promotes enantioselective addition to a reactive cationic intermediate indirectly by binding its counter-anion (Figure

^{*} Corresponding Author Jacobsen@chemistry.harvard.edu.

ASSOCIATED CONTENT

The Supporting Information is available free of charge on the ACS Publications website.

Experimental procedures, spectroscopic data, kinetic data, coordinates and energies for DFT structures (PDF)

X-Ray crystallographic data for (*ent*-**1a**)₂•hexane, (*ent*-**1a**)₂•Me₄NCl, (**1a**)•(*ent*-**1a**), (*ent*-**1b**)₂•Me₄NCl, and *epi*-**1a** (CCDC 1478172, 1478173, 1478175, 1478176, and 1478224; CIF)

1B).^{3,4} Chiral ion pairs may be accessed in a number of ways, including by catalyst-driven anion abstraction from a neutral electrophilic precursor.^{3–5}

Despite their practical attributes, chiral H-bond donors frequently exhibit low catalytic efficiency. With a few noteworthy exceptions,⁶ many H-bond donor-catalyzed reactions require high catalyst loadings (5–20 mol %) and long reaction times (>24 h). Furthermore, these catalysts are often most effective under dilute reaction conditions (0.1 M in initial substrate concentration), limiting volumetric throughput. After over a decade of investigation into the synthetic scope of these catalysts, the basis for these limitations has remained largely unknown. We reasoned that detailed mechanistic study of H-bond donor-mediated anion-binding catalysis could elucidate the origin of these limitations and thereby guide development of more efficient and broadly useful catalysts.

Toward this aim, we elected to study the enantioselective, thiourea-catalyzed alkylation of α -chloroether electrophiles with silyl ketene acetals (Scheme 1C).^{5b,7} In addition to serving as a representative model for numerous methods proposed to proceed via anion-abstraction, this reaction lends itself well to rigorous kinetic analysis due to its intermolecular nature and the fact that the active chloroether electrophile can be isolated and distilled to purity. Our analyses were conducted with both the optimal thiourea derivative (**1a**) and its urea analog (**1b**),⁸ with the goal of elucidating the similarities and differences between these H-bond donor catalyst classes.

We initiated our study with the goal of identifying the rate- and enantioselectivity-determining step(s) of the transformation. Observation of characteristic spectral features of both silyl ketene acetal **3b** and product **4b** by in situ attenuated total reflectance Fourier-transform infrared (ATR FTIR) spectroscopy enabled reaction progress kinetic analysis under synthetically relevant conditions.⁹ The excellent overlay of rate vs. concentration curves in a “same-excess” experiment demonstrated that the model system exhibits well-behaved kinetics with no appreciable catalyst deactivation, through decomposition pathways or by product inhibition, throughout the reaction (Figure 1A).¹⁰ This result has important implications, as it indicates that a more complex phenomenon must be responsible for the poor catalyst efficiency at low loading.

The kinetic order of each of the reagents was determined via “different-excess” experiments in which the initial concentration of one component was varied while the others were kept constant.⁹ The reaction displays 1st-order dependence on the concentrations of both the α -chloroisochroman electrophile, [**2**], and the silyl ketene acetal nucleophile, [**3**]. Furthermore, an inverse secondary kinetic isotope effect ($k_H/k_D = 0.87$) was observed in a competition experiment with **3c** and **3c-d₂** (Scheme 2). Taken together, these results indicate that C–C bond formation is rate- and enantioselectivity-determining. The minimal rate dependence on the identity of the silyl group of the silyl ketene acetal further suggests that desilylation occurs after the rate-determining step.¹¹

At high catalyst loading (5 mol % under the standard reaction conditions), the reaction exhibits 1st-order rate dependence on total catalyst concentration, [**1**]_T, while nonlinear behavior corresponding to low activity is observed at low catalyst concentrations (Figure

1B). This deviation from strict 1st-order behavior shed light on the low catalytic efficiency we were seeking to address, and prompted further investigation. Because a change in the kinetic order in catalyst is suggestive of aggregation,¹² the relationship between the enantiomeric purity of the catalyst and the enantioselectivity of the reaction was examined (Figure 1C). A pronounced nonlinear effect was observed, providing definitive evidence that catalyst–catalyst interaction occurs under the reaction conditions.^{12–14} As such, we sought to identify probable aggregation states and to elucidate their roles in the catalytic mechanism.

Crystallographic analysis of catalysts **1a** and **1b** reveals that discrete dimeric complexes are formed both in the presence and absence of co-crystallized tetramethylammonium chloride (Figure 2A).^{15,16} Catalysts **1a** and **1b** were also found to undergo dimerization in solution, as established through the computationally aided analysis of diagnostic nuclear Overhauser effect (nOe) correlations (Figure 2B, C).^{17–19}

Catalysts **1a** and **1b** exist as mixtures of slowly inter-converting (*E*)- and (*Z*)-amide rotamers, as determined by ¹H NMR analysis, and homodimeric (*ZZ* and *EE*) and heterodimeric (*ZE*) complexes are all detectable. A low-energy computed structure predicted for [(*Z*)-**1a**]₂ is in good agreement with the nOe correlations observed experimentally.²⁰ Both in solution and in the solid state, the dimeric structures share defining features including a “head-to-tail” arrangement, wherein the thiourea NH's of each monomer engage in H-bonding interactions with the amide oxygen of the partner molecule. The degree of aggregation was quantified by determining the dimerization constants for the (*Z*)- and (*E*)-rotamers of catalysts **1a** and **1b** by measuring changes in the chemical shifts of diagnostic ¹H NMR signals observed upon serial dilution (Figure 2C).^{21,22} Both rotameric forms of the catalysts were thus shown to exist in predominantly dimeric states under conditions relevant to catalysis.

This fact has profound implications for interpretation of the kinetic analysis described above. Because the alkylation displays a 1st-order dependence on [**1**]_T at high concentrations, the resting state and turnover-limiting transition state must possess the same, dimeric, catalyst stoichiometry under these conditions. The deviation from 1st-order dependence at low [**1**]_T can be ascribed to a change in the catalyst resting state to favor the monomer. A mechanistic model emerges wherein the catalyst is subject to a monomer–dimer equilibrium in the ground state, but where the transition state engages two molecules of catalyst. While the arrangement of the two catalyst molecules cannot be determined from the kinetic data, a plausible transition structure resembling the [(*Z*)-**1a**]₂•NMe₄Cl complex observed in the solid state is illustrated in Figure 3.²³ The kinetic data fit well to the corresponding rate law (Figure 3),^{24,25} where the fit values for *K*_{dim} are in excellent agreement with those determined by fitting NMR data (Figure 2C). Qualitatively, this rate law dictates that the reaction displays a 2nd-order kinetic dependence on catalyst concentration at low [**1**]_T and a 1st-order dependence at high [**1**]_T.

This kinetic analysis sheds light on why dual H-bond donor catalysts such as **1a** and **b** tend to be intrinsically inefficient in anion-binding pathways. At high loadings, the catalysts rest predominantly in unproductive homodimeric states.²⁶ While the catalysts rest as monomers at low loadings, each monomer must find a second catalyst molecule to engage in the anion-

binding mechanism. This insight thus lays a path for mechanism-driven improvement of catalytic activity. For example, designs for linked dimeric catalysts that favor cooperative substrate activation while avoiding nonproductive aggregation hold great promise for enabling improved catalytic efficiencies. Such linked catalysts may also provide insight into the nature of the cooperativity between the catalysts in the transition structure. Our ongoing efforts are directed toward the realization of these aims.

Supplementary Material

Refer to Web version on PubMed Central for supplementary material.

ACKNOWLEDGMENT

The authors thank Dr. S.-L. Zheng (Harvard X-Ray Laboratory) for collection and refinement of X-ray crystallographic data, Dr. Sarah E. Reisman (Caltech) and Dr. S. J. Zuend (BASF) for contributions to early stages of the project, and Dr. Eugene E. Kwan (Harvard University) for helpful discussion.

Funding Sources

The authors declare no competing financial interests. This work was supported by the NIH (GM-43214) and by fellowships to D.L. (NSERC PDF), D.D.F. (Eli Lilly and Co.) and C.R.K. (NSF DGE1144152).

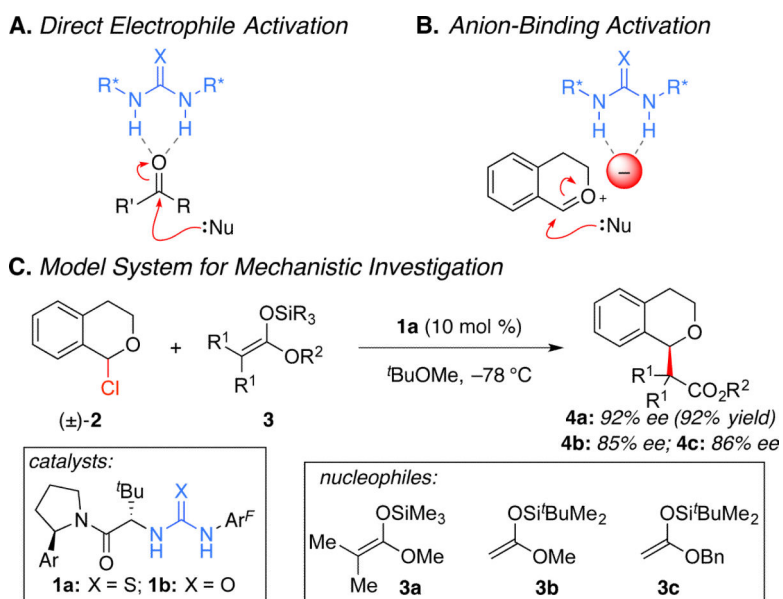
REFERENCES

1. For reviews, see: Schreiner PR. *Chem. Soc. Rev.* 2003; 32:289–296. [PubMed: 14518182] Takemoto Y. *Org. Biomol. Chem.* 2005; 3:4299–4306. [PubMed: 16327888] Connan SJ. *Chem. Eur. J.* 2006; 12:5418–5427. [PubMed: 16514689] Doyle AG, Jacobsen EN. *Chem. Rev.* 2007; 107:5713–5743. [PubMed: 18072808] Knowles RR, Jacobsen EN. *Proc. Natl. Acad. Sci. U.S.A.* 2010; 107:20678–20685. [PubMed: 20956302]
2. For select examples, see: Schreiner PR, Wittkopp A. *Org. Lett.* 2002; 4:217–220. [PubMed: 11796054] Okino T, Hoashi Y, Takemoto Y. *J. Am. Chem. Soc.* 2003; 125:12672–12673. [PubMed: 14558791] Pihko PM. *Angew. Chem. Int. Ed.* 2004; 43:2062–2064. For quantification of the LUMO-lowering effect, see: Huynh PNH, Walvoord RR, Kozlowski MC. *J. Am. Chem. Soc.* 2012; 134:15621–15623. [PubMed: 22974264] Walvoord RR, Huynh PNH, Kozlowski MC. *J. Am. Chem. Soc.* 2014; 136:16055–16065. [PubMed: 25325850]
3. For reviews, see: Zhang Z, Schreiner PR. *Chem. Soc. Rev.* 2009; 38:1187–1198. [PubMed: 19421588] Brak K, Jacobsen EN. *Angew. Chem. Int. Ed.* 2012; 52:534–561. Phipps RJ, Hamilton GL, Toste FD. *Nature Chem.* 2012; 4:603–614. [PubMed: 22824891] Beckendorf S, Asmus S, Mancheño OG. *Chem. Cat. Chem.* 2012; 4:926–936. Seidel D. *Synlett.* 2014; 25:783–794.
4. For select examples of enantioselective anion-binding catalysis with dual H-bond donors, see: Taylor MS, Tokunaga N, Jacobsen EN. *Angew. Chem. Int. Ed.* 2005; 44:6700–6704. Klausen RS, Jacobsen EN. *Org. Lett.* 2009; 11:887–890. [PubMed: 19178157] De CK, Klauber EG, Seidel D. *J. Am. Chem. Soc.* 2009; 131:17060–17061. [PubMed: 19929016] Xu H, Zuend SJ, Woll MG, Tao Y, Jacobsen EN. *Science.* 2010; 327:986–990. [PubMed: 20167783] Lin S, Jacobsen EN. *Nature Chem.* 2012; 4:817–824. [PubMed: 23000995] Mittal N, Lippert KM, De CK, Klauber EG, Emge TJ, Schreiner PR, Seidel D. *J. Am. Chem. Soc.* 2015; 137:5748–5758. [PubMed: 25871925]
5. For representative systems in which an anion-abstraction mechanism has been proposed: Raheem IT, Thiara PV, Peterson EA, Jacobsen EN. *J. Am. Chem. Soc.* 2007; 129:13404–13405. [PubMed: 17941641] Reisman SE, Doyle AG, Jacobsen EN. *J. Am. Chem. Soc.* 2008; 130:7198–7199. [PubMed: 18479086] Raheem IT, Thiara PV, Jacobsen EN. *Org. Lett.* 2008; 10:1577–1580. [PubMed: 18341346] Peterson EA, Jacobsen EN. *Angew. Chem. Int. Ed.* 2009; 48:6446–6449. Knowles RR, Lin S, Jacobsen EN. *J. Am. Chem. Soc.* 2010; 132:5030–5032. [PubMed: 20369901] Brown AR, Kuo W-H, Jacobsen EN. *J. Am. Chem. Soc.* 2010; 132:9286–9288. [PubMed: 20568761] Burns NZ, Witten MG, Jacobsen EN. *J. Am. Chem. Soc.* 2011; 133:14578–

14581. [PubMed: 21848300] Schafer AG, Wieting JM, Fisher TJ, Mattson AE. *Angew. Chem. Int. Ed.* 2013; 52:11321–11324.
6. For select examples of highly efficient, enantioselective urea- and thiourea-catalyzed transformations, see: Zuend SJ, Coughlin MP, Lalonde MP, Jacobsen EN. *Nature*. 2009; 461:968–970. [PubMed: 19829379] Birrell JE, Desrosiers J-N, Jacobsen EN. *J. Am. Chem. Soc.* 2011; 133:13872–13875. [PubMed: 21800916] For select examples of highly efficient, racemic urea- and thiourea-catalyzed transformations, see: Kotke M, Schreiner PR. *Tetrahedron*. 2006; 62:434–439. Kotke M, Schreiner PR. *Synthesis*. 2007:779–790. So SS, Burkett JA, Mattson AE. *Org. Lett.* 2011; 13:716–719. [PubMed: 21226464]
7. The alkylation of α -chloroisochroman with silyl ketene acetal nucleophiles has served as a benchmark reaction in the development of novel catalyst systems for anion-binding catalysis. For examples with halogen-bond donor anion-binding catalysts, see: Kniep F, Jungbauer SH, Zhang Q, Walter SM, Schindler S, Schnapperelle I, Herdtweck E, Huber SM. *Angew. Chem. Int. Ed.* 2013; 52:7028–7032. Jungbauer SH, Huber SM. *J. Am. Chem. Soc.* 2015; 137:12110–12120. [PubMed: 26329271]
8. Urea 1b catalyzes the formation of 4a (84 % ee), 4b (67% ee), and 4c (65% ee).
9. a Blackmond DG. *Angew. Chem. Int. Ed.* 2005; 44:4302–4320. b Blackmond DG. *J. Am. Chem. Soc.* 2015; 137:10852–10866. [PubMed: 26285166]
10. The initial concentrations $[2]_0$ and $[3b]_0$ were varied while keeping the stoichiometric excess (excess = $[3]_0 - [2]_0$) constant. See ref 9 for detailed discussion of this technique.
11. Relative rates and enantioselectivities for analogs of 3a where $\text{SiR}_3 = \text{SiMe}_3$ ($k_{\text{rel}} = 1.0$, defined; 92% ee), SiEt_3 ($k_{\text{rel}} = 0.75$, 94% ee) and $\text{Si}(\text{tPr})_3$ ($k_{\text{rel}} = 2.0$, 93% ee). For an example where a strong dependence on the identity of the silyl group was taken as evidence for rate-limiting desilylation, see ref 6b.
12. a Kagan HB. *Adv. Synth. Catal.* 2001; 343:227–233. b Blackmond DG. *Tetrahedron Asymmetry*. 2010; 21:1630–1634.
13. a Puchot C, Samuel O, Duñach E, Zhao S, Agami C, Kagan HB. *J. Am. Chem. Soc.* 1986; 108:2353–2357. [PubMed: 22175583] b Guillaenex D, Zhao S, Samuel O, Rainford D, Kagan HB. *J. Am. Chem. Soc.* 1994; 116:9430–9439. c Satyanarayana T, Abraham S, Kagan HB. *Angew. Chem. Int. Ed.* 2009; 48:456–494.
14. Both reservoir effects and catalyst cooperativity in the enantioselectivity-determining step likely contribute to the net nonlinear effect. For further discussion, see the Supporting Information.
15. The crystal structures shown in Figure 2A were obtained with catalyst ent-1a instead of 1a. The mirror images of those structures are presented here.
16. Dimeric and oligomeric complexes of some urea and thiourea catalysts have been reported. For select examples, see: Etter MC, Urbańczyk-Lipkowska, Zia-Ebrahimi M, Panunto TW. *J. Am. Chem. Soc.* 1990; 112:8415–8426. Taylor MS, Tokunaga N, Jacobsen EN. *Angew. Chem. Int. Ed.* 2005; 44:6700–6704. ^c ref 4f.
17. For a review of intermolecular NOESY, see: Mo H, Pochapsky TC. *Prog. Nucl. Mag. Res. Sp.* 1997; 30:1–38.
18. Frisch MJ, et al. Gaussian 09, Revision A.01. 2009 Gaussian Inc. Wallingford, CT See Supporting Information for full citation.
19. a Becke AD. *J. Chem. Phys.* 1993; 98:5648–5652. b Lee C, Yang W, Parr RG. *Phys. Rev. B.* 1988; 37:785–789. c Miehlich B, Savin A, Stoll H, Preuss H. *Chem. Phys. Lett.* 1989; 157:200–206. d Frisch MJ, Pople JA, Binkley JS. *J. Chem. Phys.* 1984; 80:3265–3269.
20. Computed structures consistent with the nOe correlations observed for [(E)-1a]₂ and (E)-1a•(Z)-1a are described in the Supporting Information.
21. a Tan HKS. *J. Chem. Soc., Faraday Trans.* 1994; 90:3521–3525. b Nogales DF, Ma J-S, Lightner DA. *Tetrahedron*. 1993; 49:2361–2372.
22. For discussion of the relative rates of amide bond rotation and dimerization, see the Supporting Information.
23. Plausible alternatives include an arrangement in which one thiourea molecule forms H-bonds to the S of the other catalyst molecule, thereby increasing its chloride-binding ability. For examples and discussion of conceptually similar interactions, see: Jones CR, Panto GD, Morrison AJ, Smith

MD. *Angew. Chem. Int. Ed.* 2009; 48:7391–7394. Probst N, Madarász Á, Valkonen A, Pápai I, Rissanen K, Neuvonen A, Pihko PM. *Angew. Chem. Int. Ed.* 2012; 51:8495–8499. Auvil TJ, Schafer AG, Mattson AE. *Eur. J. Org. Chem.* 2014:2633–2646. ^d ref 4f.

24. A similar kinetic scenario has been identified in epoxide opening with fluoride, catalyzed by (salen)Co complexes. See: Kalow JA, Doyle AG. *J. Am. Chem. Soc.* 2011; 133:16001–16012. [PubMed: 21863842]
25. Intermediate catalyst–substrate complexes are likely formed rapidly and reversibly en route to the rate-determining alkylation transition state. Because the concentrations of these fleeting intermediates are negligible (i.e. the total catalyst concentration in the rate law can be described as $[1]_T \sim [1] + 2[1 \bullet 1]$), they have no kinetically meaningful impact on the overall rate law for the reaction.
26. The kinetic data alone do not distinguish whether dimer $1 \bullet 1$ is on- or off-cycle. However, the catalyst self-aggregation mode determined crystallographically, spectroscopically, and computationally effectively masks the H-bonding functionality necessary to promote the reaction. We posit that this aggregate must dissociate either partially or completely in order to engage the substrate.



Scheme 1.
Enantioselective, H-bond donor-mediated anion-binding catalysis.

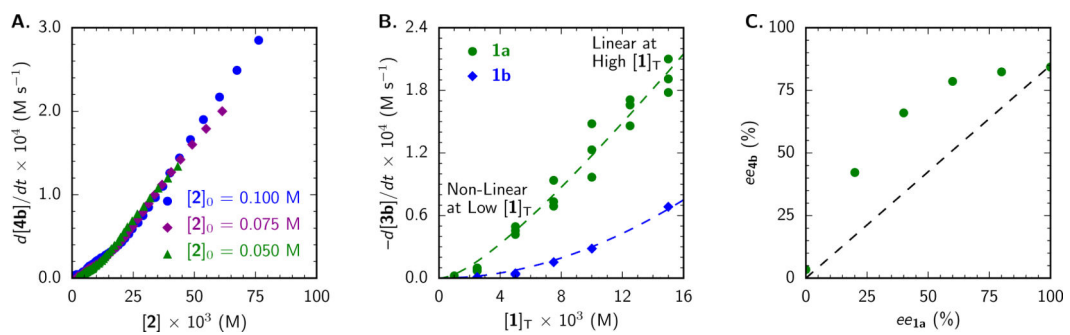
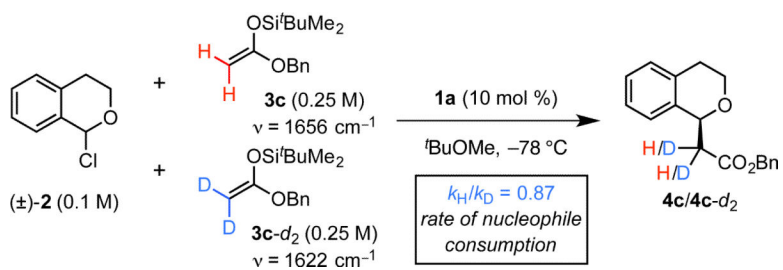
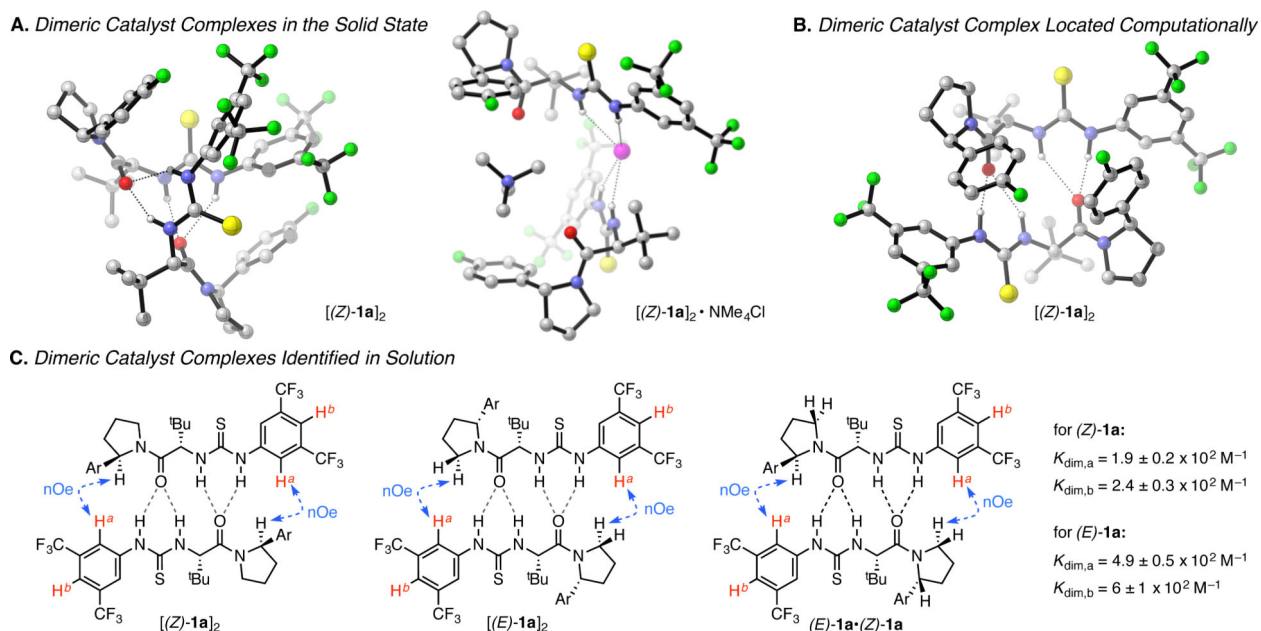


Figure 1.

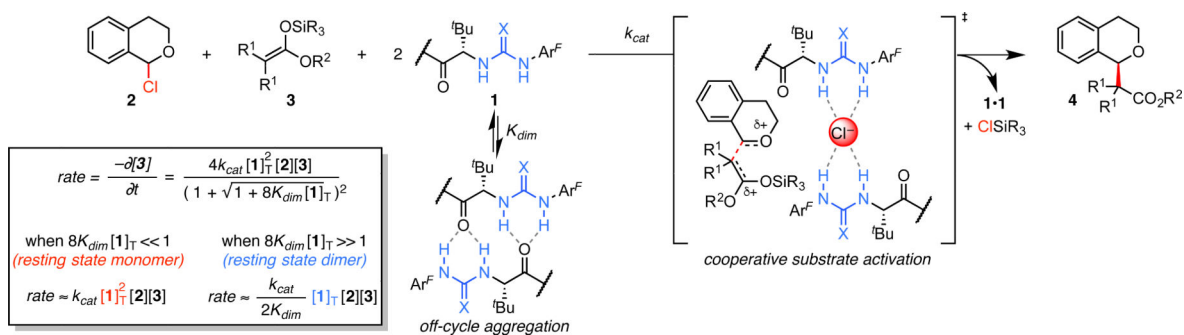
A. Same-excess experiment with $[1a]_T = 0.01$ M. B. Dependence of alkylation rate (at 30% conv) on $[1]_T$, fit to the rate law in Figure 3. C. Nonlinear relationship between product ee and catalyst ee . See Supporting Information for details.



Scheme 2.
Kinetic isotope effect.

**Figure 2.**

A. X-ray crystallographic structures of **1a** in the absence (left) and presence (right) of co-crystallized NMe₄Cl. B. Low-energy ground-state dimeric complex of **1a** identified computationally (B3LYP/6-31G(d,p)). C. Head-to-tail dimers of **1a** identified by 2D NOESY NMR in toluene-*d*₈ at 23 °C. Key nOe correlations utilized to assign these structures are labeled in blue, while the resonances monitored to determine the dimerization constants of (*Z*)-**1a** and (*E*)-**1a** are indicated in red. Experimental details and the corresponding data for urea **1b** are provided in the Supporting Information. Ar = 4-fluorophenyl

**Figure 3.**

Proposed mechanism for the enantioselective, H-bond donor-catalyzed alkylation of α -chloroisochroman. The rate law derived from this mechanistic picture accounts for the kinetic behavior shown in Figure 1B. The fit parameters for catalysts **1a** and **1b** are, as follows: with **1a**, $k_{\text{cat}} = 4.6 \pm 1.9 \times 10^2 \text{ M}^{-3} \text{ s}^{-1}$, $K_{\text{dim}} = 94 \pm 56 \text{ M}^{-1}$, $R^2 = 0.97$; with **1b**, $k_{\text{cat}} = 39 \pm 9 \text{ M}^{-3} \text{ s}^{-1}$, $K_{\text{dim}} = 1.6 \pm 4.5 \text{ M}^{-1}$, $R^2 = 0.987$. See ref 24.